

THE ROLE OF NEGATIVE BUOYANCY IN SURFACE-BASED CONVECTION AND ITS REPRESENTATION IN CUMULUS PARAMETERIZATION SCHEMES

Manisha Ganeshan*¹ and Raghu Murtugudde^{1,2}

¹Department of Atmospheric and Oceanic Science, University of Maryland, College Park, MD

²Earth System Science Interdisciplinary Center, University of Maryland, College Park, MD

1. INTRODUCTION

Even with recent advances in computational capabilities and numerical weather forecasting, the modeling of convective processes continues to pose a challenge to the scientific community. Some widely prevalent biases, observed in regional and global climate models alike, include a poor representation of the phase and amplitude of warm season rainfall. For example, the characteristic late-afternoon peak associated with daytime surface-based convection is predicted to occur too early during morning hours. (e.g., Betts and Jakob 2002; Dai and Trenberth 2004; Lee et al. 2007; Dirmeyer et al. 2010). In their study, Dai and Trenberth (2004) speculated that weak thermodynamic constraints on CIN may be responsible for the rather effortless initiation of daytime convection. Cumulus parameterization schemes trigger deep convection based on large-scale dynamical constraints, other than purely thermodynamic considerations of parcel buoyancy. For example, some convective schemes use the grid-resolved moisture flux convergence (Kuo 1974), or the temporal change in the large-scale convective available potential energy (CAPE; Arakawa and Schubert 1974) as convective triggers. Some other schemes, such as the Tiedtke and Kain-Fritsch (KF), explicitly check for parcel buoyancy in the sub-cloud layer but impose less stringent constraints above this level. Typically, moist convection in cumulus parameterization schemes is allowed to begin from the lifting condensation level (LCL) as opposed to the level of free convection (LFC). This will be discussed in more detail with respect to the Betts-Miller-Janjić (BMJ) and the Kain-Fritsch (KF) scheme later in the paper.

Apart from biases, considerable discrepancies exist between popular cumulus parameterization schemes. Liang et al. (2004) compared the performance of the Grell and KF schemes in simulating the diurnal cycle of warm season precipitation over the continental US. They observed that the KF scheme, which triggers convection based on buoyancy constraints, works better

in simulating the daytime peak of surface-based convection observed over the Southeast US. Whereas, the Grell scheme, which is primarily based on the quasi-equilibrium assumption, is capable of capturing the nocturnal phase of warm season rainfall over the Great Plains region (Liang et al. 2004). Thus, the convective trigger in cumulus parameterization schemes is usually a complex function consisting of a combination of dynamic and thermodynamic constraints. These constraints may work favorably for a particular region and a particular type of convection versus another.

This study investigates the role of negative buoyancy (or CIN) in the triggering of surface-based convection, and compares its representation in two popular cumulus parameterization schemes (BMJ and KF). Model simulations are carried out over the Chesapeake Bay watershed where the nature of late-afternoon convection during the warm season is expected to be surface-based (Wallace 1975; Colman 1990). The model runs are tested for sensitivity to horizontal resolution, treatment of convection (cumulus scheme on/off), boundary layer physics and cumulus physics. In addition to model analyses, the importance of negative buoyancy in initiating surface based convection in the real atmosphere is examined using satellite-derived soundings. The experimental procedure is described in the next section, followed by a discussion of major results (section 3) and a summary of our findings (section 4).

2. METHODS

2.1 *Design of experiments and model set-up*

Six warm season surface-based precipitation events of 1-2 day duration occurring over the Chesapeake Bay watershed in a conditionally unstable atmosphere (negative lifted index values), with rainfall beginning around 1200-1400 LST, are selected. Analyses of surface and upper-air meteorology for each event is carried out using synoptic weather maps obtained from the Hydrometeorological Prediction Center (HPC) of the National Weather Service, and Unisys weather. Table 1 provides a list of meteorological conditions observed across the region on each rain day, along with fronts at 0800 LST.

* *Corresponding Author Address:* Manisha Ganeshan, Department of Atmospheric and Oceanic Science, University of Maryland, College Park, MD 20742-2425; e-mail: mganeshan@atmos.umd.edu

Event	Diurnal Max. Temp. (°C)	Dewpoint Temp. at 0800 LST (°C)	Lifted Index at 0800 LST (°C)	Fronts at 0800 LST
<i>Aug 4-5, 2010</i>				
Day1	25-33	21-24	0 to -4	Surface trough oriented N-S
Day2	28-33	19-23	-2 to -4	Approaching cold front from NW
<i>Jun 8-9, 2009</i>				
Day1	27-29	17-20	0 to -2	Stationary front oriented E-W
Day2	27-31	19-21	-2 to -6	Squall line oriented N-S
<i>May 24, 2009</i>				
Day1	22-30	15-18	0 to -4	Approaching cold front from NW
<i>Jun 3-4, 2008</i>				
Day1	23-29	12-16	2 to -2	Approaching cold/stationary front from NW
Day2	27-29	18-21	0 to -5	Warm front oriented E-W
<i>Aug 25-56, 2007</i>				
Day1	29-37	21-24	-2 to -8	No surface fronts
Day2	30-38	20-25	0 to -4	Cold front oriented NE-SW
<i>July 5-6, 2005</i>				
Day1	30-33	19-22	0 to -3	Approaching cold front from W
Day2	29-33	20-23	0 to -2	Stationary front oriented N-S

*Lifted Index is defined as the difference in environmental temperature and parcel temperature at 500hPa.

TABLE 1. The range of observed meteorological conditions over the Chesapeake Bay watershed.

The control experiment consists of nested runs using the Weather Research and Forecast (WRF) model (Skamarock et al. 2008) at three different resolutions, viz., coarse (37.5 km), medium (7.5 km) and fine (2.5 km) resolutions. The domain and the one-way nesting configuration of the model are shown in Figure 1. The cumulus parameterization scheme is activated for the coarse and the medium resolution nested grids only, whereas the fine grid resolves convection explicitly. The model output is evaluated over the shaded region (shown in Fig. 1) at all three resolutions. This enables us to examine the sensitivity of our results not only to horizontal resolution but also to the treatment of cumulus physics. The control experiment is carried out using the Betts-Miller-Janjić (BMJ) cumulus parameterization scheme (Betts 1986; Betts and Miller 1986; Janjić 1994) and the Yonsei University (YSU) boundary layer scheme (Hong et al. 2006). The BMJ scheme uses a convective adjustment method, and activates deep convection if the cloud-depth exceeds 200 hPa. Although it doesn't explicitly consider parcel buoyancy in its trigger function, it includes an implicit constraint for cloud-layer CIN based on enthalpy conservation (Baldwin et al. 2002).



FIG 1. Model experimental domain (shaded) over the Chesapeake Bay watershed, shown along with the three-grid nesting configuration that is used. The outermost grid resolution is 37.5 km, the middle grid is 7.5 km and the innermost grid resolution is 2.5 km.

The model has 30 vertical levels in the terrain-following sigma coordinate system from the surface to 100 hPa. The unified Noah Land Surface Model (Chen and Dudhia 2001) predicts heat and moisture fluxes at the surface while the WRF Single-Moment 5-class (WSM5)

scheme (Hong et al. 2004; Hong and Lim 2006) is chosen for parameterizing microphysics. Two sets of sensitivity experiments are carried out, first by replacing the YSU with Mellor-Yamada-Janjić (MYJ) boundary layer scheme (Mellor and Yamada 1982), and the second by replacing the BMJ with the KF cumulus parameterization scheme (Kain 2004).

The Global Forecast System (GFS) model is used for initial and boundary conditions. In the past, studies involving long-term climate modeling experiments have reported the problem of premature convection. One reason for using the GFS model to drive WRF is to investigate whether similar timing errors also exist in “forecast” mode (i.e., when no data assimilation is active). For each event, a lead time of at least 12 hours is allowed for model spin-up. In addition to the control run, 4 more ensemble runs are created by perturbing initial temperature and moisture values within the lower atmospheric levels (from the surface up to the lowest six sigma levels). It is expected that surface-based convection will be most sensitive to perturbations at these levels. The perturbations are computed using a random normal distribution function with mean = 0, and standard deviation = 1.8 °K (for temperature) and 10% (for relative humidity). It is ensured that points of supersaturation are not produced.

2.2 Validation against observations

The 4.7 km resolution Stage IV precipitation dataset from the National Centers for Environmental Prediction’s Environmental Modeling Center (NCEP’s EMC) (Baldwin and Mitchell 1996; Lin and Mitchell 2005) is used as observational reference primarily to verify the modeled diurnal cycle of precipitation during each event. Satellite-derived soundings from the Atmospheric Infrared Sounder (AIRS) instrument onboard the National Aeronautics and Space Administration’s (NASA’s) Aqua Spacecraft is used to investigate relevant trigger processes. The AIRS Level 1B infrared, geolocated, and calibrated radiances product is used. Since atmospheric soundings from ground-based sources (radiosondes, aircraft profiles, etc.) are not available at sufficient spatio-temporal frequency, the high spatial resolution (13.5km) AIRS dataset is employed. Hyperspectral soundings of temperature and moisture are obtained at 101 levels using separate clear-sky (Weisz et al. 2007a) and cloudy (Weisz et al. 2007b) regression retrieval algorithms. Satellite pass occurs over the Chesapeake Bay watershed in the afternoon (between 1300–1500 LST), which is around the time of precipitation onset. Profiles of temperature and moisture are obtained over locations with observed rainfall recorded soon after the satellite pass. This provides a snapshot of the real

atmosphere just prior to the initiation of convection. A suitable cloud filter (Smith et al. 2012) is used to include pixels with clear-sky or optically thin cloud conditions only. After applying this filter, the retrieval algorithms produce soundings that are fairly realistic. For example, a comparison with radiosonde observations for a convective event over South Africa suggests that AIRS is able to successfully capture the observed spatial variability in the vertical structure of the atmosphere (Fig.2). This gives us confidence that the high spatial information contained in this dataset is indeed usable to study location-specific soundings over grid points with observed rainfall.

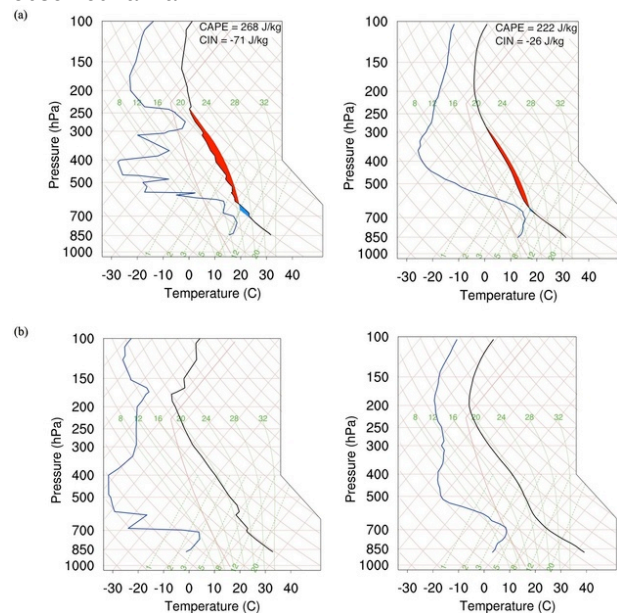


FIG 2. Comparison of co-located skew T-log P soundings obtained from radiosonde (IGRA) measurements at 1000 UTC (L), and AIRS satellite data at 1135 UTC (R) using (a) cloudy regression retrieval algorithm over Pretoria and (b) clear-sky regression retrieval algorithm over De Aar. The soundings are recorded on November 28, 2006 during a warm season convective event that occurred in South Africa.

2.3 Convective and Pre-convective soundings

The regression retrieval is performed over grid points that have precipitation beginning at a time closest to, but soon after the satellite pass (1400-1600 LST). These atmospheric profiles represent the soundings of the convective atmosphere, as they are observed right before convection occurs. Similarly, profiles are also retrieved over grid points with rainfall beginning two hours after satellite pass (1600-1800 LST). These time-

lagged profiles may be referred to as soundings of the pre-convective atmosphere. The observed differences between convective and pre-convective soundings are used to infer processes that are relevant to the triggering of surface-based convection.

The step-wise procedure to obtain these representative skew T-log P soundings is described below.

- 1.) Using Stage IV gridded precipitation, locations with observed rainfall beginning within the hour or next of satellite pass (i.e. 1400-1600 LST) are identified. Latitude and longitude values of these locations are obtained.
- 2.) This information is used to co-locate corresponding location indices within the AIRS satellite granule.
- 3.) Retrievals of temperature and moisture profiles are obtained at these locations using the regression algorithms, and skew T-log P soundings representative of the convective atmosphere are generated. (Points with cloud contaminated retrievals or non-positive surface CAPE are disregarded).
- 4.) The above steps are repeated for locations with observed precipitation beginning approximately two hours after satellite pass (1600-1800 LST). The soundings from these grid points are used as a proxy to represent the pre-convective atmosphere.

As an example, Figure 3(a) shows the satellite-derived land surface temperature over our region of interest retrieved using the clear-sky regression algorithm, on August 5, 2010 (1447 LST).

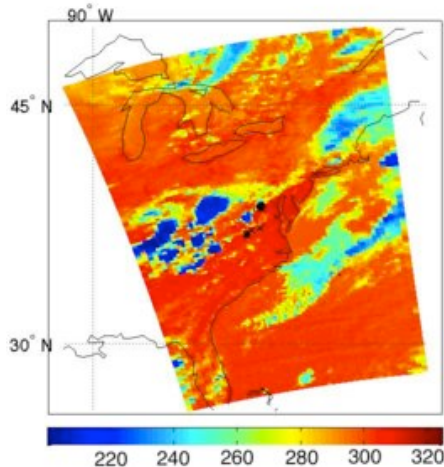


FIG 3. (a) Satellite-derived land surface temperature (°K) on August 5, 2010 at 1447 LST, shown along with locations used for retrieving atmospheric soundings representing the convective atmosphere (grid point marked with '•' sign) and pre-convective atmosphere (grid points marked with 'x' sign).

The point marked with a black '•' sign indicates a location with precipitation beginning between 1400-1500 LST, that is used to obtain temperature and moisture profiles representative of the convective atmosphere (see Fig. 3 (b)). Similarly, grid points with precipitation beginning between 1600-1700 LST are marked with black 'x' signs in Figure 3 (a). These are subsequently used to retrieve soundings of the pre-convective atmosphere. Note that retrievals at the hour closest to observed rainfall are not as abundantly available due to contamination by clouds. The skew T-log P thermodynamic charts discussed in this study are obtained using the NCAR Command Language (NCL version 6.0) software (2012).

3. RESULTS

3.1 *The Diurnal cycle of mean rainfall and thermodynamic parameters*

Figure 4 compares the temporal evolution of the domain-averaged ensemble mean precipitation at each resolution with observations. It can be seen that the onset and peak of convection occurs too early in the parameterized grids (left panels of Fig. 4 (a)-(f)). Moreover, the sensitivity to model resolution remains low when convection is parameterized. Explicit convection does not always improve the mean precipitation but it appears to rectify the early bias and thereby improve the temporal evolution of rainfall (companion panels of Fig. 4 (a)-(f)). Thus, the premature triggering of convection is most likely due to deficiencies in the cumulus parameterization scheme. Baldwin et al. (2002) have identified certain characteristic features produced by the BMJ scheme's shallow convective mechanism that may erroneously eliminate the capping inversion or CIN, which is crucial in suppressing surface-based deep convection. The scheme's shallow convection does not include any constraints on negative buoyancy, and is easily triggered as long as there is CAPE in the atmosphere. It causes warming and drying near the cloud-base but cooling and moistening near the cloud-top. This mixing process consequently removes stable layers or negative buoyancy thus allowing deep convection to occur easily (Baldwin et al. 2002). In order to inspect whether this is responsible for the early onset of convective rainfall, the diurnal cycle of CAPE and CIN is compared between parameterized and explicit grids (Fig. 5). While there is no major difference in the phase, some amplitude differences do exist. The CIN however, is higher during the initiation of parameterized convective rainfall suggesting that there is no significant contribution to premature precipitation by the BMJ scheme's shallow convection. In fact, the relatively high CIN values at the time of rainfall onset indicate that the deep convective trigger function is unable to recognize

the presence of a moderate to strong capping layer during morning hours. The convective adjustment in the scheme only produces precipitation if there is a net warming and drying within the cloud, thus automatically imposing an implicit constraint on negative buoyancy (CIN) in its trigger for deep convection (Baldwin et al. 2002). Baldwin et al. (2002) posit that in the presence of

strong CIN or a stable inversion layer above the LCL, the adjustment process will entail extensive cooling and moistening thereby failing to initiate deep convection. It appears that such an implicit trigger may not be sufficient to suppress convection. This is further investigated using model soundings in subsection 3.4.

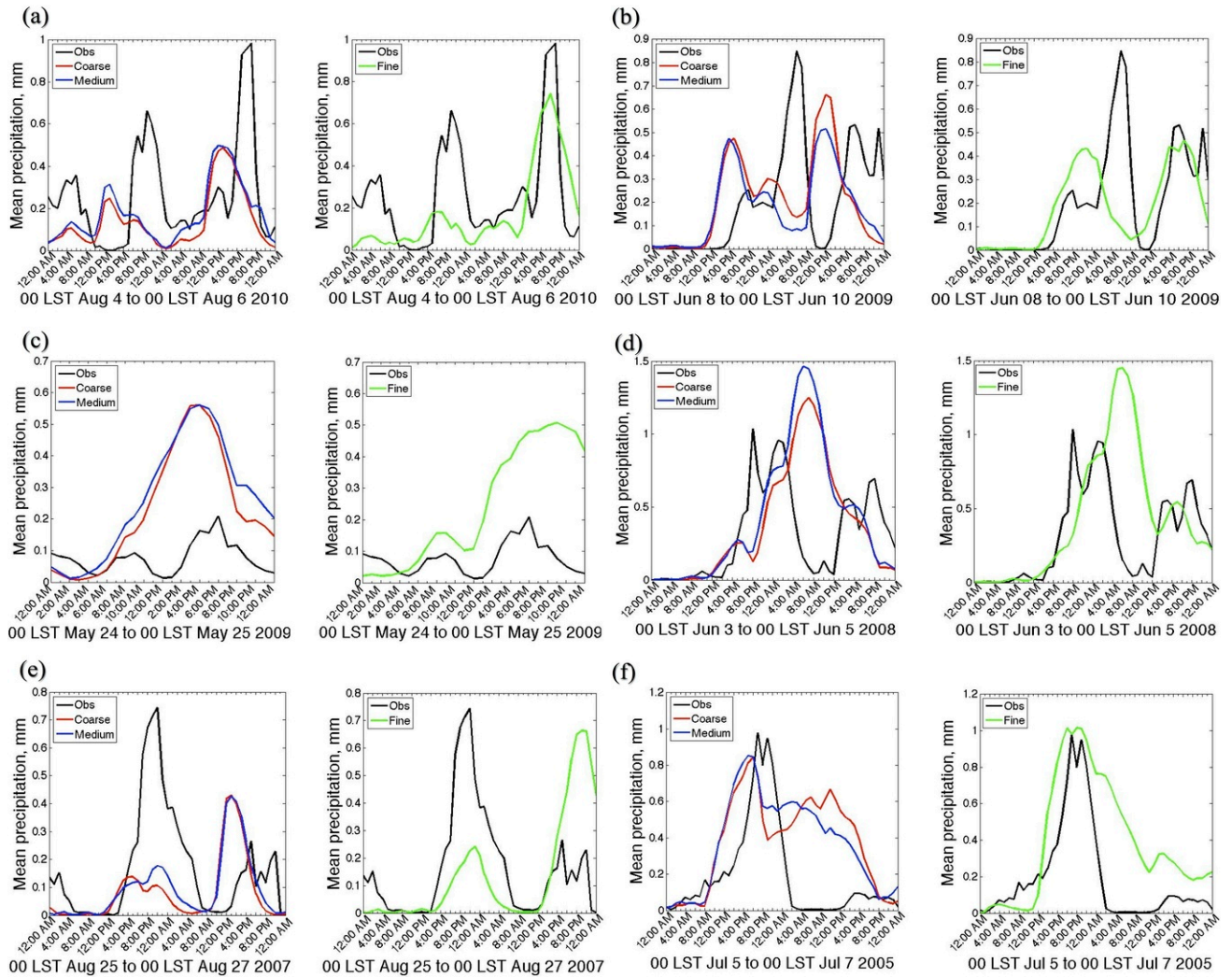


FIG 4. Temporal evolution of ensemble mean precipitation forecasts for coarse (red), medium (blue) and fine (green) resolutions against observations (black) on (a) August 4-5, 2010, (b) June 8-9, 2009, (c) May 24, 2009, (d) June 3-4, 2008, (e) August 25-26, 2007 and (f) July 5-6, 2005

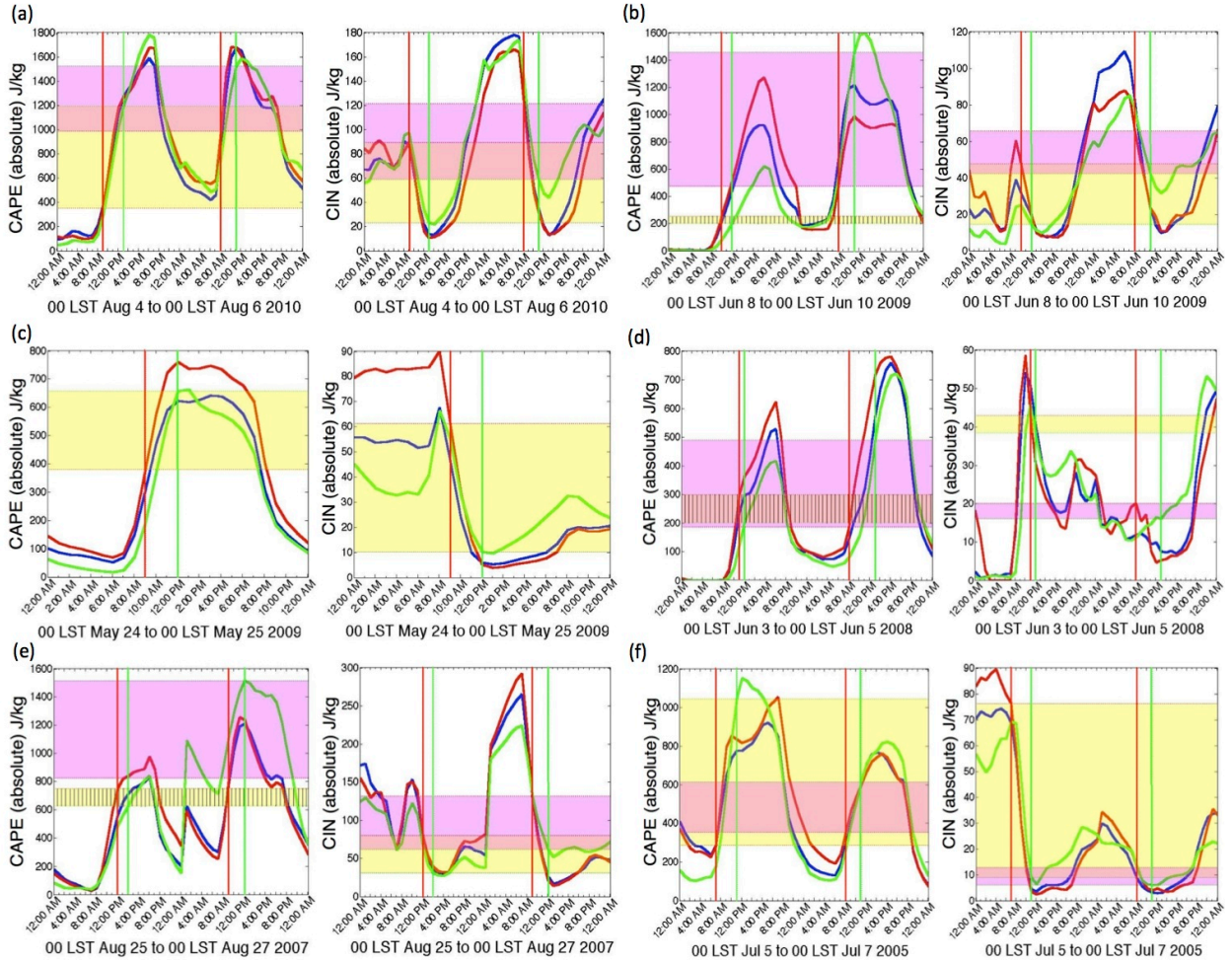


FIG 5. Temporal evolution of ensemble mean absolute CAPE (positive buoyancy) and absolute CIN (negative buoyancy) averaged over grid points with precipitation for coarse (red), medium (blue) and fine (green) resolutions on (a) August 4-5, 2010, (b) June 8-9, 2009, (c) May 24, 2009, (d) June 3-4, 2008, (e) August 25-26, 2007 and (f) July 5-6, 2005. The colored vertical lines represent the timing of onset of deep convection within the coarse (red) parameterized and fine (green) explicit grids. The yellow and magenta shading represent buoyancy differences between coarse and fine grids observed during convective initiation on the first and second days of the events, respectively. Differences in positive buoyancy are calculated by subtracting the absolute mean CAPE values of coarse grid from that of fine grid ($ICAPE_{fine} > ICAPE_{coarse}$). Differences in negative buoyancy are calculated by subtracting the absolute mean CIN values of fine grid from that of coarse grid ($ICIN_{coarse} > ICIN_{fine}$). Negative differences are hatched.

3.2 Sensitivity to Model Physics

Results from the sensitivity experiment using the MYJ boundary layer scheme are compared with output from the control run for parameterized grids. The temporal evolution of the mean precipitation from the control (red) and sensitivity (blue) runs shows very little

divergence for the coarse grid (see left panels of Figures 6(a)-(f)). The model solution is more sensitive to cumulus physics as indicated by the output from the second set of sensitivity experiments performed using the KF cumulus parameterization scheme (see right panel of Fig.6 (a)-(f)). Similar results are also obtained

for the medium (7.5km) grid (not shown). The early bias in the onset of parameterized convection however, persists when the KF scheme is used. This warrants an investigation of the KF scheme's trigger function in addition to that of the BMJ scheme. In a following subsection (3.4), co-located model soundings within the parameterized and explicit grids are compared and

plausible reasons for the premature onset of parameterized convection in both schemes is discussed. It is, however, useful to first inspect the characteristics of observed atmospheric soundings obtained prior to the start of convection.

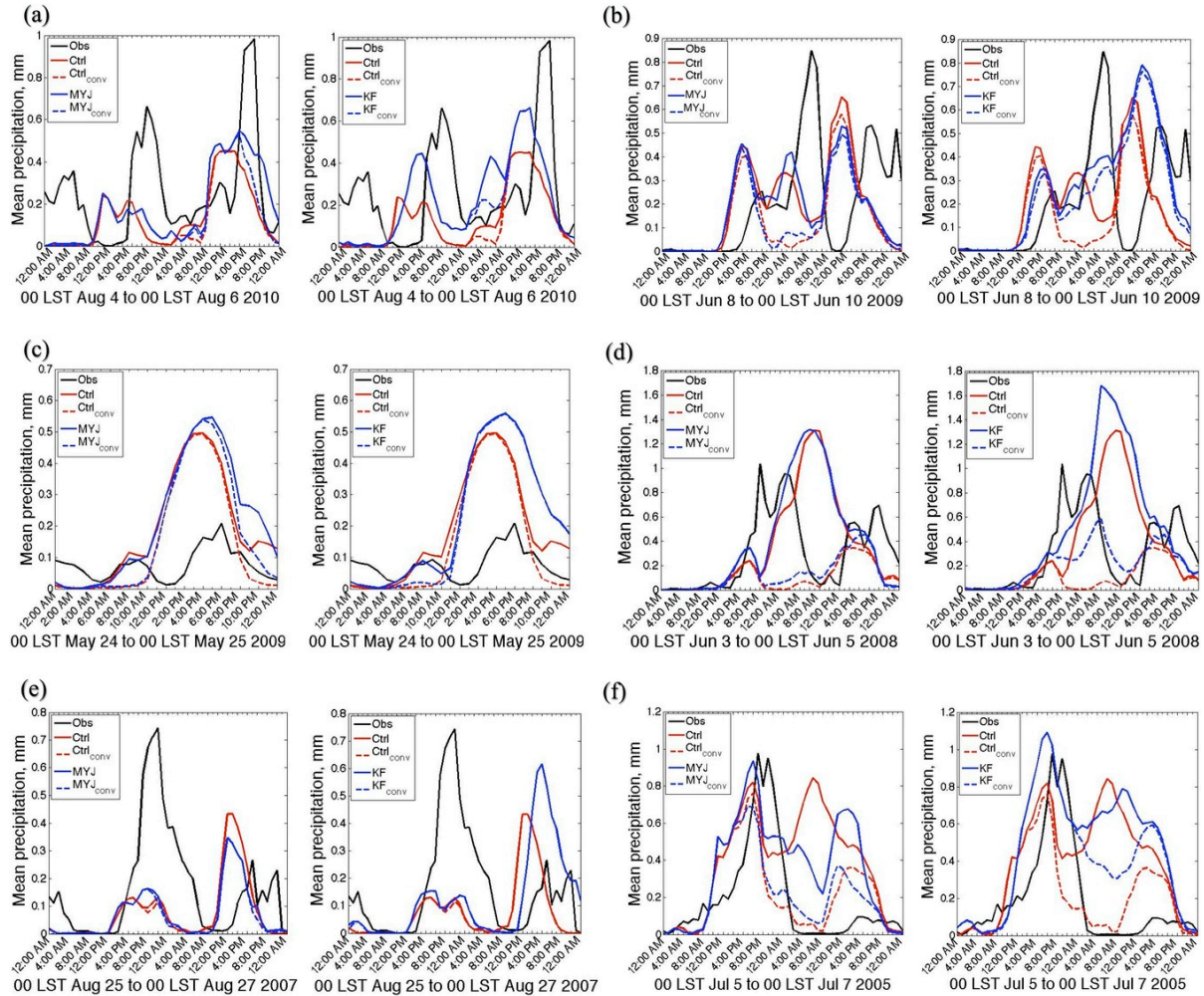


FIG 6. Mean precipitation forecast at coarse (37.5km) resolution from control run (red), sensitivity run (blue) against observations (black) on (a) August 4-5, 2010, (b) June 8-9, 2009, (c) May 24, 2009, (d) June 3-4, 2008, (e) August 25-26, 2007 and (f) July 5-6, 2005. For each subfigure, the sensitivity run using MYJ boundary layer scheme is shown in the left panel, and the sensitivity run using KF cumulus parameterization scheme is shown in the right panel. The dotted lines represent the convective component of mean precipitation produced by control run (red) and sensitivity run (blue).

3.3 Atmospheric Soundings

Convective soundings are obtained at grid points with rainfall recorded at the hour closest to satellite pass. As a result, cloud contamination becomes a

significant problem. For most cases, only a single representative clear-sky or (thin) cloudy retrieval sounding is obtained. No data are available for Aug 4, 2010, May 24, 2009, Jun 3-4, 2008 and Jul 6, 2005. In

all soundings observed on the remaining rain days, there is negligible CIN and conditions are favorable for the development of surface-based convection. The left and center panels of Fig.7 compares the pre-convective and convective soundings obtained on two days. Note that there are no mesoscale boundaries in the vicinity of rainfall during the first case (Aug 25, 2007), but convection occurs ahead of an approaching westerly cold front during the second event (Aug 05, 2010). The convective soundings in Fig.7 have near-saturated relative humidity (RH) values at the surface and a well-developed boundary layer thus indicating that the necessary thermodynamic forcing mechanisms for surface-based convection are present. Although high

surface RH is also evident in the corresponding pre-convective soundings, the presence of CIN between the LCL and LFC appears to delay rainfall. The planetary boundary layer (PBL; 1000-850 hPa) structural differences between the two soundings (right panel of Fig.7) suggest that vertical mixing and development of an unstable lapse rate are important factors for the removal of CIN. Such a layer of negative buoyancy is conspicuously absent in all soundings of the convective atmosphere. Thus, satellite observations confirm that negative buoyancy between the LCL and LFC is indeed a necessary trigger constraint for the occurrence of surface-based deep convection.

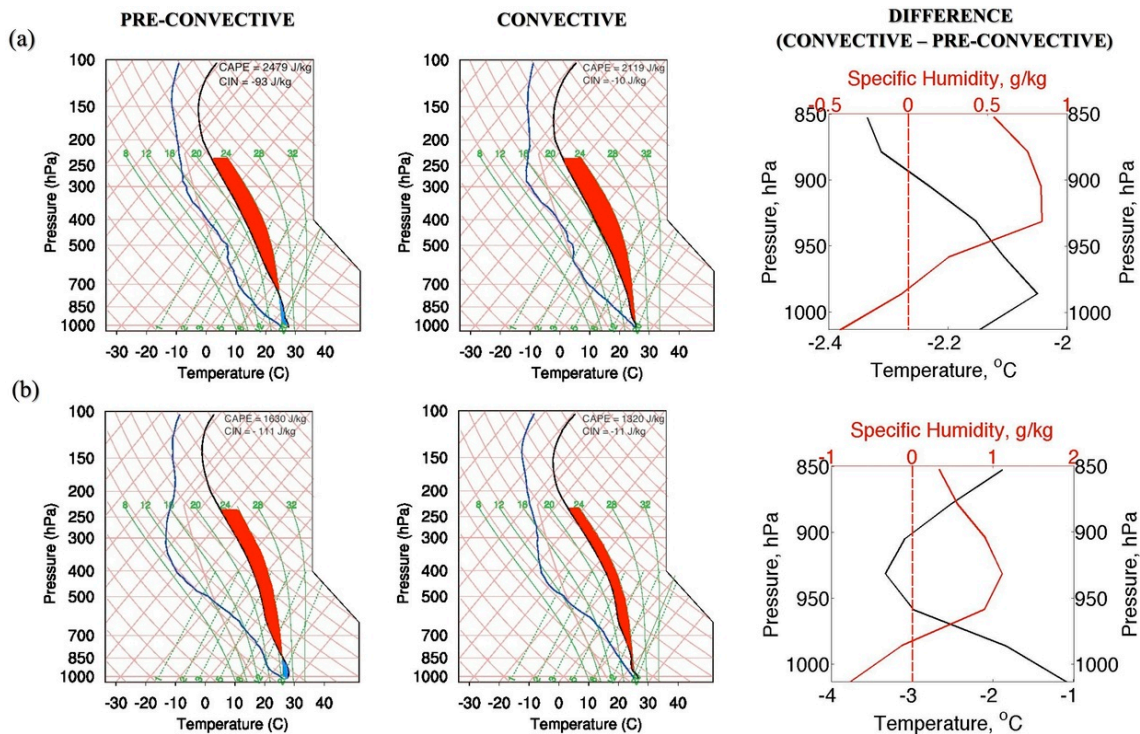


FIG 7. Satellite-derived clear-sky soundings obtained over locations with precipitation (accumulated) beginning at 1700 LST (L) and 1500 LST(C) along with the PBL (1000-850 hPa) differences between the two soundings (R) on (a) Aug 25, 2007, and (b) Aug 05, 2010. Satellite pass occurs over the Chesapeake Bay watershed at 1441 LST on Aug 25, 2007 and at 1447 LST on Aug 05, 2010.

3.4 Model Soundings

Model soundings at grid points with early parameterized convection are compared against co-located soundings from the explicit grid at the time of convective initiation. (Only grid points with convective to total precipitation ratio in excess of 0.9 are selected). At

the hour of early rainfall, it is evident that the layer of negative buoyancy above the LCL inhibits explicit convection but fails to suppress the occurrence of parameterized convection. The left and center panels of Figure 8 show examples of model soundings from co-located grid points in the coarse (37.5km) and fine

(2.5km) grids, obtained at the time of premature convection by the BMJ scheme. There is negative buoyancy between the LCL and LFC at this time, but clearly the implicit constraint on CIN imposed by the

scheme is insufficient to suppress deep convection. Explicit convection begins later during the day only after the convective boundary layer and the instability are well developed (right panels of Fig.8).

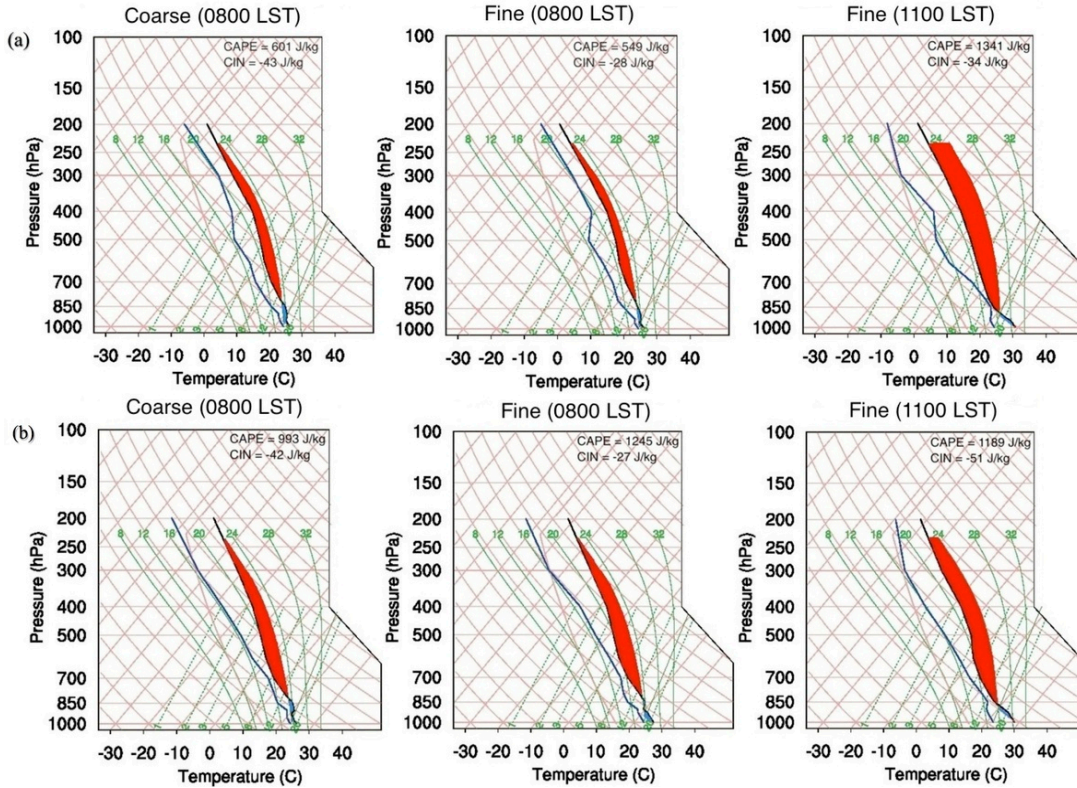


FIG 8. Skew T-log P soundings obtained over co-located grid points at the hour of initiation of parameterized convection in the coarse (L) and fine (M) grids, and at the hour of initiation of explicit convection in the fine grid (R) for (a) August 5, 2010; and (c) July 5, 2005. Parameterized convection begins at 0800 LST while explicit convection begins at 1100 LST on both days. The soundings in this figure are obtained from the control run using BMJ scheme.

Similar to Figure 8, the left and center panels of Figure 9 show examples of co-located soundings obtained from the sensitivity run using the KF scheme, at the time of onset of parameterized convection. Once again, there is negative buoyancy below the LFC. This layer of CIN is unable to suppress parameterized deep convection, although it delays explicit convection which begins only after the CIN is overcome (right panel of Fig.9 (a),(b)). The trigger for moist convection in the KF scheme, unlike the BMJ scheme, explicitly accounts for CIN by using a parcel buoyancy equation, but applying it only at the LCL (cloud-base). The scheme first forms a well-mixed updraft source layer (USL) starting from the lowest model level up to a layer-depth of at least 60hPa.

The USL is raised to its LCL at which point a perturbation temperature (δT), proportional to the grid-resolved vertical velocity at that level (w_g), is assigned to it (see Eq.1). The term c_z refers to a threshold vertical velocity in cm s^{-1} , which is proportional to the height of the LCL, and k is a unit number with dimensions $^\circ\text{K s}^{1/3} \text{cm}^{-1/3}$. For details on calculation of c_z , refer to Kain (2004).

$$\delta T = k[w_g - c_z]^{1/3} \quad (1)$$

Moist convection, or the formation of convective updrafts is allowed if the sum of the parcel temperature and δT , exceeds the environmental temperature at the LCL. This means that even for a

slightly positive large-scale vertical velocity (the order of a few centimeters per second), a marginally stable parcel at its cloud-base can become a convective updraft. (Note that theoretically, moist convection may occur only when the parcel is able to reach its LFC, not LCL). The constraint described above appears to be satisfied for the case of the soundings shown in Figure 9 (left panel), since the parcel is nearly neutral at the LCL and a small perturbation may easily make it positively buoyant. This, in fact, is true for both soundings. The vertical velocity (w_g) computed at the cloud-base is found to be small but positive, viz., 1.24 and 2.5 cm s^{-1}

respectively. The resulting temperature perturbation calculated from Eq.1 will then be around 1 and 1.25 $^\circ\text{K}$, respectively, which is sufficient to satisfy the buoyancy criteria at the cloud-base. After the decision to activate moist (shallow/deep) convection is made, the USL (now updraft) is released with its original unperturbed temperature and moisture properties at the LCL, and with a vertical velocity given by Eq.2. The terms Z_{LCL} and Z_{USL} refer to the heights of the LCL and base of the USL, respectively, while T_{ENV} refers to the temperature of the environment at LCL.

$$w_{p0} = 1 + 1.1 [(Z_{\text{LCL}} - Z_{\text{USL}}) * \delta T / T_{\text{ENV}}]^{1/2} \quad (2)$$

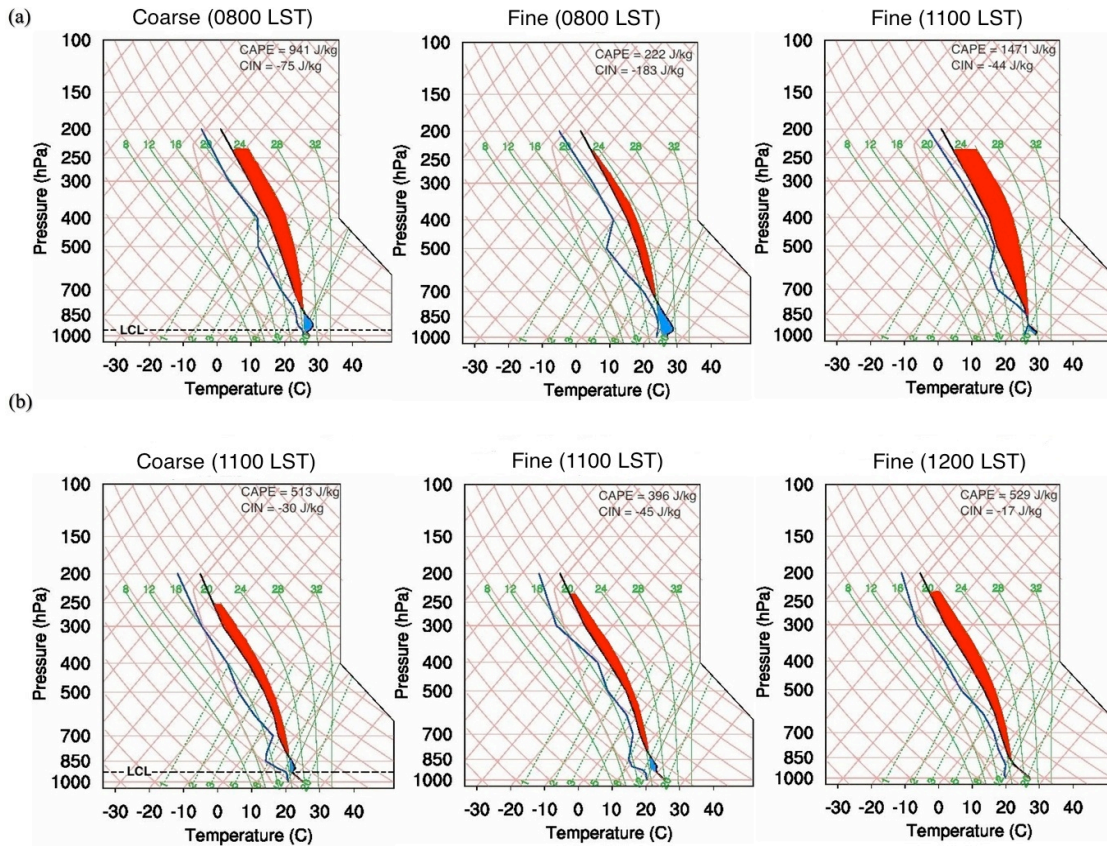


FIG 9. Skew T-log P soundings obtained over co-located grid points at the hour of initiation of parameterized deep convection in the coarse (L) and fine (M) grids, and at the hour of initiation of explicit convection in the fine grid (R) for (a) August 5, 2010 and (b) June 8, 2009. Parameterized convection begins at 0800 LST for sounding in (a) and at 1100 LST for sounding in (b), whereas explicit convection begins at 1100 LST for sounding in (a) and at 1200 LST for sounding in (b), respectively. The soundings in this figure are obtained from the control run using KF scheme.

According to Kain (2004), the above formula yields starting velocities up to several meters per second. Thus, the parcel that was marginally buoyant at the LCL,

is now a full-fledged convective updraft with a significantly positive vertical velocity. For the soundings shown in Figure 9, Eq.2 approximately yields vertical

velocities (w_{po}) of 2 and 2.4 $m s^{-1}$, respectively, which is two orders of magnitude greater than the original vertical velocity (w_g) at the LCL. The scheme then simulates the ascent of the convective updraft in the cloud using the Lagrangian parcel method, including constraints of entrainment, detrainment and water loading (Kain 2004). Kain (2004) claims that these constraints act as additional trigger criteria for deep moist convection above the LCL by determining whether or not the required minimum cloud depth (2-4km) is achieved. The updraft may be prevented from reaching this minimum depth criterion if entrainment of environmental air causes it to become negatively buoyant within the cloud. While this may be true, such a formulation to account for negative buoyancy above the LCL can hardly be considered as an “explicit trigger”. Consider the sounding shown in the left panel of Figure 9(b). Immediately above the LCL, the convective updraft rises through layers of negative buoyancy and dry environmental relative humidity where detrainment dominates, and the entrainment rate is expected to be only a minimum as opposed to maximum (Kain 2004). In such a case, clearly the dilution with the environmental air does not actively work to “inhibit” the updraft from reaching its LFC. Thus, it appears that the present considerations for parcel buoyancy above the LCL do not qualify as an effective trigger for deep convection. The decision to activate moist convection or convective updrafts at the LCL, prior to accounting for CIN above it, is a common assumption in other schemes as well (Tiedtke 1989, Fritsch and Chappell 1980). Not only does this assumption fail to suppress deep convection, it may also produce overactive shallow convection.

Sometimes, the updraft may reach the LFC through layers of negative buoyancy but is unable to fulfill the minimum depth criterion. In this case, the scheme may activate shallow convection, which brings about mixing within the cloud and preconditions it for the occurrence of deep convection at a later time. Such an example is shown in Figure 10. The sub-cloud layer shows similar properties for both parameterized and explicit grids. However, it appears that shallow convection has removed the negative buoyancy above the LCL (seen in right panel of Fig.10), thereby enabling easy triggering of deep convection in the parameterized grid at this hour (left panel of Fig.10). This is analogous to the effect of shallow convection in the BMJ scheme reported by Baldwin et al. (2002), and appears to contribute to premature and overactive convection. Thus, it appears that the negative buoyancy above the LCL needs more stringent or explicit considerations, and must be accounted for *prior* to the triggering of moist (both shallow and deep) convection.

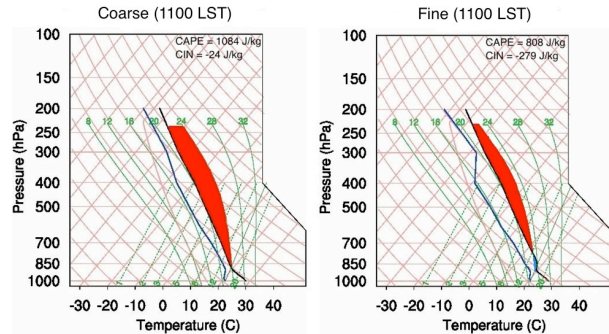


FIG 10. Skew T-log P soundings obtained over co-located grid points in the coarse (L) and fine (R) grids at the hour of initiation of parameterized deep convection (1100 LST) on Aug 26, 2007. The sounding in this figure is obtained from the sensitivity run using KF scheme.

3.5 Preliminary Experiments with modified KF scheme

In order to investigate KF scheme’s sensitivity to the negative buoyancy above cloud-base, a modification is made such that moist convection begins only when the LCL and LFC are at the same pressure level (difference less than 1hPa). Preliminary results suggest that such a modification may help in reducing errors in the diurnal cycle. For the same two cases discussed in Fig.7, a comparison is made between model runs (37.5km resolution) using the original and the modified KF schemes. In addition, comparison is also made with a model run using the KF scheme but with a revised large-scale trigger. This large-scale trigger is based on the grid-resolved three-dimensional moisture advection (Ma and Tan 2009) as opposed to the vertical velocity that is used in the original scheme (Kain 2004).

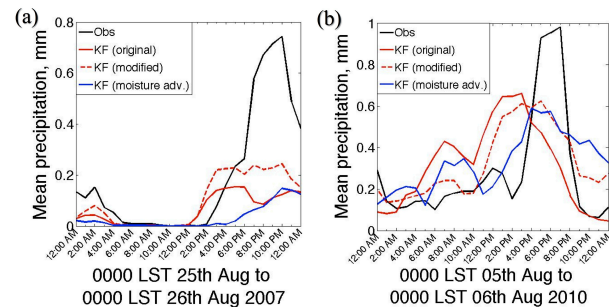


FIG 11. The diurnal cycle of mean precipitation for (a) Aug 25, 2007; and (b) Aug 05, 2010 obtained using Stage IV observations (black), the original Kain-Fritsch scheme (red), the modified Kain-Fritsch scheme (red, dotted) and the Kain-Fritsch scheme with revised large-scale trigger (blue).

For the first case with no surface fronts, both the large-scale triggers are unable to capture the convective peak (Fig.11a). The modified KF scheme marginally improves the amplitude. For the second case (Fig.11b), the modified scheme delays the initiation as well as peak of convection, thereby improving the overall representation of the phase. By accounting for CIN, the discrepancies between the two large-scale triggers are reduced. This modified scheme is also tested in a climate simulation for the year 2009 (Jun-Aug) using initial and boundary conditions from the North American Regional Reanalysis (NARR; Mesinger et al. 2006). Preliminary comparisons suggest that accounting for CIN may improve the representation of the phase propagation associated with Mesoscale Convective Systems (MCSs) across the Central Plains region (see Fig.12).

4. SUMMARY

This study explored the role and representation of negative buoyancy in triggering surface-based convection using two popular cumulus parameterization schemes, viz. the Betts-Miller-Janjic (BMJ) and the Kain-Fritsch (KF) schemes. Both schemes trigger moist convection from the LCL (not LFC), assuming implicit constraints for CIN above it. As a result, they fail to suppress overactive morning convection. It appears that the biases in the phase and amplitude of warm season rainfall may be reduced by explicitly accounting for CIN between the LCL and LFC. Although large-scale processes will remain crucial for triggering parameterized convection, more stringent constraints on the negative buoyancy may help reduce the discrepancies between different cumulus parameterization schemes.

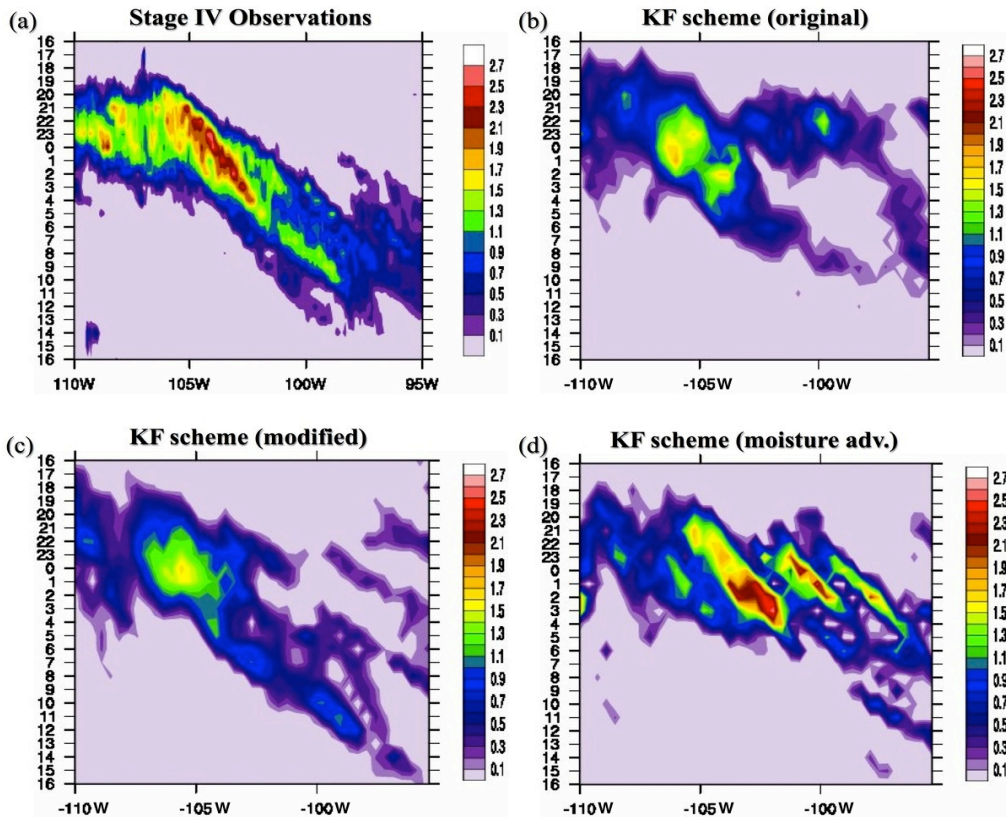


FIG 12. Hovmöller diagram of normalized rainfall diurnal variations averaged between 38–42°N for (a) Stage IV observations, and for model output using (b) the original Kain-Fritsch scheme, (c) the modified Kain-Fritsch scheme, and (d) the Kain-Fritsch scheme with revised large-scale trigger based on moisture advection.

REFERENCES

- Arakawa, A., and W. H. Schubert, 1974: Interaction of a cumulus cloud ensemble with the large-scale environment, part I. *J. Atmos. Sci.*, **31**, 674 – 701.
- Baldwin, M. E., and K. E. Mitchell, 1996: The NCEP hourly multi-sensor U.S. precipitation analysis. Preprints, *11th Conference on Numerical Weather Prediction, Norfolk, VA*.
- _____, J. S. Kain, and M. P. Kay, 2002: Properties of the convection scheme in NCEP's Eta Model that affect forecast sounding interpretation. *Wea. Forecasting*, **17**, 1063-1079.
- Betts, A. K., 1986: A new convective adjustment scheme. Part I: Observational and theoretical basis. *Quart. J. Roy. Meteor. Soc.*, **112**, 677–691.
- _____, and M. J. Miller, 1986: A new convective adjustment scheme. Part II: Single column tests using GATE wave, BOMEX, and arctic air-mass data sets. *Quart. J. Roy. Meteor. Soc.*, **112**, 693–709.
- _____, and C. Jakob, 2002: Evaluation of the diurnal cycle of precipitation, surface thermodynamics, and surface fluxes in the ECMWF model using LBA data. *Journal of Geophysical Research*, **107**, D20, 8045, doi:10.1029/2001JD000427
- Chen, F., and J. Dudhia, 2001: Coupling an advanced land-surface/ hydrology model with the Penn State/ NCAR MM5 modeling system. Part I: Model description and implementation. *Mon. Wea. Rev.*, **129**, 569–585.
- Colman, B. R., 1990: Thunderstorms above frontal surfaces in environments without positive CAPE. Part I: A climatology. *Mon. Wea. Rev.*, **118**, 1103–1122.
- Dai, A. F., and K. E. Trenberth, 2004: The Diurnal Cycle and its Depiction in the Community Climate System Model. *Journal of Climate*, **17**, 930-95.
- Dirmeyer, P. A., and Coauthors, 2010: Simulating the hydrologic diurnal cycle in global climate models: Resolution versus parameterization. A Technical Report from Center for Ocean-Land-Atmosphere Studies, American Meteorological Society, **304**, 45 pp.
- Fritsch, J. M., and C. F. Chappell, 1980: Numerical prediction of convectively driven mesoscale pressure systems. Part 1: Convective parameterization. *J. Atmos. Sci.*, **37**, 1722-1733.
- Hong, S., J. Dudhia, and S. Chen, 2004: A Revised Approach to Ice Microphysical Processes for the Bulk Parameterization of Clouds and Precipitation. *Mon. Wea. Rev.*, **132**, 103–120.
- _____, Y. Noh, and J. Dudhia, 2006: A new vertical diffusion package with an explicit treatment of entrainment processes. *Mon. Wea. Rev.*, **134**, 2318–2341.
- _____, and J. J. Lim, 2006: The WRF Single-Moment 6-Class Microphysics Scheme (WSM6). *Journal of the Korean Meteorological Society*, **42**, 129–151.
- Janjić, Z. I., 1994: The step-mountain eta coordinate model: further developments of the convection, viscous sublayer and turbulence closure schemes. *Mon. Wea. Rev.*, **122**, 927–945.
- _____, 2004: The Kain-Fritsch Convective Parameterization: An Update. *Journal of Applied Meteorology*, **43**, 170-181
- Kuo, H.-L., 1974: Further studies of the parameterization of the influence of cumulus convection on large-scale flow. *J. Atmos. Sci.*, **31**, 1232– 1240.
- Lee, M., and Coauthors, 2007: An Analysis of the Warm-Season Diurnal Cycle over the Continental United States and Northern Mexico in General Circulation Models. *Journal of Hydrometeorology*, **8**, 344-366.
- Liang, X., L. Li, A. Dai, and K. E. Kunkel, 2004: Regional climate model simulation of summer precipitation diurnal cycle over the United States. *Geophysical Research Letters*, **31**, L24208, doi:10.1029/2004GL021054.
- Lin, Y., and K. E. Mitchell, 2005: The NCEP Stage II/IV Hourly Precipitation Analyses: Development and Applications. Proceedings, *19th AMS Conference on Hydrology, San Diego, CA*.
- Ma, L-M. and Tan Z-M, 2009: Improving the behavior of cumulus parameterization for tropical cyclone prediction: Convective trigger. *Atmospheric Research*, **92**, 190-211.

Mellor, G. L., and T. Yamada, 1982: Development of a turbulence closure model for geophysical fluid problems. *Rev. Geophys. Space Phys.*, **20**, 851–875.

Mesinger, F. and Coauthors, 2006: North American Regional Reanalysis. *Bull. Amer. Meteor. Soc.*, **87**, 343-360.

Skamarock, W. C., and Coauthors, 2008: A description of the Advanced Research WRF version 3. NCAR Tech Note NCAR/TN-475+STR, 113 pp.

Smith, W. L., E. Weisz, S. Kirev, D. K. Zhou, Z. Li, and E. E. Borbas, 2012: Dual-regression retrieval algorithm for realtime processing of satellite ultraspectral radiances. *J. Appl. Meteor. Climatol.*, **51**, 1455–1476.

Tiedtke, M., 1989: A comprehensive mass flux scheme for cumulus parametrization in large-scale models. *Mon. Wea. Rev.*, **117**, 1779–1800.

Wallace, J. M., 1975: Diurnal variations in precipitation and thunderstorm frequency over the conterminous United States. *Mon. Wea. Rev.*, **103**, 406–419.

Weisz, E., H.-L. Huang, J. Li, E. Borbas, K. Baggett, P. Thapliyal, and L. Guan, 2007a: International MODIS and AIRS processing package: AIRS products and applications. *Journal of Applied Remote Sensing*, **1**, 013519.

_____, J. Li, D. K. Zhou, H.-L. Huang, M. D. Goldberg, P. Yang, 2007b: Cloudy sounding and cloud-top height retrieval from AIRS alone single field-of-view radiance measurements. *Geophysical Research Letters*, **34**, L12802.